Environmental Science Nano

Titanium dioxide and table sugar enhance the leaching of silver out of nanosilver packaging

Journal:	*Environmental Science: Nano*
Manuscript ID	EN-ART-02-2023-000098.R1
Article Type:	Paper

Titanium dioxide and table sugar enhance the leaching of silver out of nanosilver packaging

Tianxi Yang[1†‡], Laxmi Adhikari[1‡], Teena Paulose[2], Reiner Bleher[3], and Timothy V. Duncan[1*]

[1]Center for Food Safety and Nutrition, US Food and Drug Administration, Bedford Park IL, 60501

[2]Department of Food Science and Nutrition, Illinois Institute of Technology, Bedford Park IL, 60501

[3]Department of Materials Science and Engineering and the Northwestern University Atomic and Nanoscale Characterization Experimental (NUANCE) Center, Northwestern University, Evanston, IL 60208

*Corresponding author: timothy.duncan@fda.hhs.gov

[†]Current affiliation: Food Nutrition and Health Program, Faculty of Land and Food Systems, University of British Columbia, Vancouver, BC V6T 1Z4, Canada

Environmental significance statement

Nanosilver has received intense interest as an additive to plastic packaging due to its antimicrobial properties. Ensuring the safety of these materials in potential food contact applications requires fully understanding factors that determine migration of silver into foods under intended use conditions. Here we show that table sugar and the whitening agent TiO_2 cooperatively enhance the transfer of silver out of nanosilver-enabled plastics, and they also shift the balance of ionic and particulate silver present in the contacted environment. These findings imply that using simple food simulants like purified water in experimental migration assessments may underpredict the amount of silver likely to be found in real foods stored within nanosilver packaging materials.

Titanium dioxide and table sugar enhance the leaching of silver out of nanosilver packaging

Tianxi Yang[1†‡], Laxmi Adhikari[1‡], Teena Paulose[2], Reiner Bleher[3], and Timothy V. Duncan[1*]

[1]Center for Food Safety and Nutrition, US Food and Drug Administration, Bedford Park IL, 60501

[2]Department of Food Science and Nutrition, Illinois Institute of Technology, Bedford Park IL, 60501

[3]Department of Materials Science and Engineering and the Northwestern University Atomic and Nanoscale Characterization Experimental (NUANCE) Center, Northwestern University, Evanston, IL 60208

*Corresponding author: timothy.duncan@fda.hhs.gov

[†]Current affiliation: Food Nutrition and Health Program, Faculty of Land and Food Systems, University of British Columbia, Vancouver, BC V6T 1Z4, Canada

[‡]Contributed equally to this work

Abstract. We manufactured laboratory-scale food packages containing 2.57 ± 0.18 $\times 10^{-3}$ wt % silver nanoparticles (AgNPs) and used them to show that table sugar (sucrose) and microcrystalline titanium dioxide (μTiO_2) enhance Ag migration from these packages and into aqueous food simulants. Ag migration into purified water was detected but was below the limit of ICP-MS quantitation, giving a range of potential Ag migration between 0.059 and 0.082 ng/cm^2 packaging surface area. Ag migration into 9 wt % aqueous sucrose solution was 0.547 ± 0.084 ng/cm^2 and migration into 9 wt % sucrose solution containing 0.01 wt % μTiO_2 was 0.724 ± 0.032 ng/cm^2. Total Ag migration into a 0.01 wt % μTiO_2 aqueous dispersion without sucrose was between 0.122 and 0.162 ng/cm^2, with upper and lower limits defined by the detectability of Ag in the supernatant phase of the simulant. If the midpoint of this range is taken as a baseline, these results imply that, compared to purified water, Ag migration was increased by approximately 10.3 times when the water simulant contained μTiO_2 and sucrose at commercially-relevant concentrations. Notably, the Ag migrated into water containing both ingredients exceeded the total Ag migrated into either of the single-ingredient simulants, pointing to a potential cooperative relationship between sucrose and μTiO_2 that possibly derives from binding and redox interactions between these two ingredients. Sucrose and μTiO_2 also both reduced a portion of migrated Ag^+ back into AgNPs, and μTiO_2 particles efficiently captured (>25 % by mass) migrated Ag on their surfaces. Similar effects

on migration were observed with nanocrystalline TiO_2. These experiments are the first to show that TiO_2 particles exert a strong influence on the quantity and form of Ag that could migrate from AgNP-enabled packaging, suggesting that food formulations and interactions between individual food components may be important to consider when evaluating the fate of nanoparticles in these consumer applications.

Keywords: food, titanium dioxide, silver nanoparticles, migration, packaging, exposure

INTRODUCTION

Polymer nanocomposites (PNCs) are widely thought to be promising materials for next generation food packaging. Incorporated nanomaterials imbue polymers with a diverse range of attributes, including improved strength and toughness, sensing capability, and reduced oxygen and water vapor permeability.[1,2] PNCs based on silver nanoparticles (AgNPs) have received especially heightened interest due to their strong antimicrobial properties.[3-7] Deploying AgNP-containing food contact polymers in consumer products faces significant challenges, however. Chief among these is uncertainty with respect to whether embedded AgNPs may migrate to foods.[8-15] Studies have established that migration of Ag mass into food simulating substances from AgNP-enabled plastics commonly occurs under long term storage conditions, but there is still a poor understanding of polymer-, nanoparticle-, or food-specific factors that may influence either the amount or form of Ag to which consumers could ultimately be exposed. Pre-market authorization of AgNP-based food packaging is required in many countries (including the United States) to ensure that such materials are safe under their intended conditions of use. An important element in establishing the safety of AgNP-based food packaging is the evaluation of AgNP migration. Therefore, fully characterizing AgNP migration pathways and defining appropriate migration test protocols is a critical aspect of the product development pipeline.

Migration of Ag from AgNP/polymer packaging to contacted foods and beverages is chiefly driven by a two-step process. First, oxygen permeates the polymer and oxidizes the surfaces of dispersed AgNPs; second, the oxidized AgNPs slowly shed Ag, which diffuses to the external environment along a concentration gradient. Factors that enhance (or suppress) AgNP surface oxidation correspondingly influence the total migrated Ag mass. For example, we have shown that Ag migration is sensitive to the initial AgNP diameter (surface area), the AgNP

composition, and the oxygen content of the storage medium.[15] Released silver mass can theoretically present in two forms: nanoparticulate or dissolved ionic silver.[16] Ionic silver appears to dominate the leachate when migration experiments are performed in simple aqueous or acidic food simulants. On the other hand, we recently demonstrated that certain reducing ingredients commonly found in foods and beverages (e.g., monosaccharide sugars), or ingredients that can hydrolyze into reducing substances during storage (starches or complex sugars), are capable of converting ionic Ag migrated from packaging back into particulate Ag with various sizes and morphologies.[17] Because ionic and particulate Ag may exhibit different biological effects after oral exposure,[18] these prior findings suggest that the way in which food and beverage ingredients influence the fate of nanoparticulate food packaging additives should be further explored.

The motivating goal of this study was to determine whether titanium dioxide (TiO_2) exerts a strong influence on AgNP migration behavior. TiO_2 is used as an additive in some foods and beverages to brighten their white color.[19,20] TiO_2 has been reported in commercial sweetened and unsweetened beverages and semi-liquid foods in the United States at concentrations ranging from 3.59 μg/mg Ti (coconut curd, ~0.6 wt % TiO_2) down to 8.92×10^{-2} μg/mLTi (sweetened pineapple beverage, ~1.5×10^{-5} wt % TiO_2).[21] TiO_2 has also been observed in European food products, including animal- and plant-based milks, yogurt, sugary beverages, and salad dressings.[22] TiO_2 exists primarily in two different crystal structures (anatase and rutile), and both forms have been detected in pristine food grade TiO_2 pigments and commercial food products.[23-25] Food grade TiO_2 typically exhibits primary crystallite sizes below 100 nm, although crystallite size distributions can be quite large and TiO_2 particles in practice frequently manifest as aggregates with sizes considerably larger than the individual crystallite dimensions, often on the scale of hundreds of nm.[25] Current United States regulations permit the use of TiO_2 in foods up to 1 wt %, although certain other restrictions exist with respect to allowed impurity levels, labeling requirements, and so on.[26]

Our hypothesis that TiO_2 might influence Ag migration from AgNP/polymer PNCs derives from extensive literature on the complex interactions between metal oxide particles and metal ions in solution. For instance, TiO_2 can act as an adsorbent for heavy metals,[27-29] including Ag.[30-32] Under illumination, photogenerated electrons at TiO_2 surfaces can efficiently reduce ionic Ag into particulate Ag, and most of the formed Ag particles remain adsorbed onto or incorporated within

the TiO_2 surface layers.[32-34] Alternatively, TiO_2 could produce reactive oxygen species (ROS) such as hydroxyl and superoxide radical anions,[35] which promote the oxidization and dissolution of particulate Ag into ionic Ag.[33] As such, we theorized that TiO_2 at concentrations relevant to its use as a food additive might enhance Ag migration from AgNP-loaded polymers and/or catalyze post-migration morphological transformations between Ag^+ and AgNPs. Additionally, carbohydrates, including mono-, di-, and polysaccharides, form strong interactions with TiO_2 particles in aqueous solution under various conditions. These interactions give rise to changes in TiO_2 hydrodynamic diameter, surface charge, colloidal stability, and physicochemical behaviors.[36-39] TiO_2 can also photocatalyze the degradation of surface-bound carbohydrates (include sucrose) or their conversion into other redox reactive chemicals.[38,40-42] As such, we hypothesized that TiO_2 may act in concert with table sugar or other common redox-active food substances to bring about cooperative effects on Ag migration from AgNP-enabled plastics.

We tested these hypotheses first by studying interactions between TiO_2 particles, sucrose, and different concentrations of Ag in aqueous solution in the absence of packaging materials. After incubating these mixtures, the Ag form was characterized (e.g., Ag-TiO_2 complex, unbound AgNPs, and unbound Ag^+) using UV-Visible spectroscopy, X-ray diffraction, and electron microscopy when the initial Ag concentration was high and using inductively coupled plasma mass spectrometry (ICP-MS) in standard mode and single particle mode (SP-ICP-MS) when the Ag concentration was low. We then manufactured miniature packages (sachets) out of AgNP-loaded low density polyethylene (LDPE), which was produced from commercial polymer resin and laboratory-synthesized AgNPs. Aqueous food simulants containing combinations of TiO_2 and/or sucrose (a representative sugar) at commercially relevant concentrations were stored in these sachets under accelerated room temperature storage conditions, and the simulants were then characterized by ICP-MS and SP-ICP-MS to determine the quantity and form of Ag migrated under these conditions.

METHODS

Materials. Silver nitrate ($AgNO_3$, 99.9999%), trisodium citrate dihydrate (TSC, ≥ 99%), tannic acid (ACS reagent), poly(ethylene glycol) methyl ether thiol (PEG-thiol, average Mn 2,000), chloroform ($CHCl_3$, 99.5%), and low-density (poly)ethylene (LDPE, MW ≈ 80 kDa, density = 0.925 g/mL, melt index = 25 g/10 min, Lot#: MKCB9440) were purchased from

Millipore Sigma. Sucrose was purchased from Fisher Scientific (BP/EP/NF Pharmaceutical grade, product S2, refined from cane) and from Millipore Sigma (sucrose (BioXtra ≥99.5%, GC, refined from cane). Both laboratory grade sucrose products are refined cane sugars; the sucrose from Millipore Sigma was used for μTiO_2 migration experiments; all other experiments used the sucrose purchased from Fisher. Hydrochloric acid (HCl, 32−35%, Optima grade) and nitric acid (HNO_3, 67−70%, Optima grade) were purchased from Fisher Scientific. ICP silver standards (1000 ± 4 μg/mL in 4 % HNO_3, density = 1.020 g/mL @ 20.1°C) were purchased from SCP Science. AgNP reference material (NanoXact citrate-capped silver nanospheres, 50 nm nominal particle diameter, product number: AGCN50-25M) was purchased from nanoComposix. Inc. Microcrystalline titanium (IV) oxide (μTiO_2, rutile, 99.9+ %) and nanocrystalline titanium (IV) oxide ($nTiO_2$, nanopowder, rutile, 99.5 %) were purchased from Aldrich Chemical Company. All water used in this study was UV-sterilized and purified to a resistance of 18.2 MΩ cm using a Millipore-Sigma MilliQ Direct Q3 water purification system. All sonication of dispersions in this study was accomplished using a Bransonic 2510R 100W ultrasonic bath cleaner.

Interactions between TiO_2 particles and Ag^+ at high Ag concentration. Aqueous suspensions (15 mL) containing 0.5 mM $AgNO_3$ and either 0.05 wt % $nTiO_2$ or 0.05 wt % μTiO_2 were prepared in glass scintillation vials (Fisher scientific) with plastic caps. Control solutions with only $AgNO_3$ but no TiO_2 and with neither $AgNO_3$ nor TiO_2 were also prepared. Additionally, a series of four samples with 9 wt % aqueous sucrose solution in place of water were prepared. These eight solutions were placed in a Thermo Max Q4000 orbital shaker set to 60 RPM and stored under ambient room light at 40 °C for a period of 10 days. At select time intervals the samples were removed and photographed using a Samsung S22 smart phone camera. At 4 hours and 24 hours, 100 μL aliquots were removed from the TiO_2-containing samples for electron microscopy analysis. The supernatants were also periodically removed with a pipette and characterized by UV-Visible spectroscopy; these supernatants were returned to the vials after measurement. Finally, at 10 days the TiO_2 precipitates were isolated by centrifugation (3600 rpm/2738 rcf, 5 minutes), washed twice with water with repeated centrifugation, and analyzed by X-ray diffraction (XRD). Details on UV-visible, electron microscopy, and XRD measurements are provided in the Supporting Information section.

Interactions between TiO_2 particles and Ag^+ at low Ag concentration. Aqueous suspensions (50 mL) containing either μTiO_2 of $nTiO_2$ particles (0.05 wt%) and Ag^+ (0.25 or 2.5

μg/L) were stored in plastic tubes (50 mL tubes, SCP Science) under ambient light or in the dark. Ag^+ in these solutions was diluted from an Ag^+ standard (1000 μg/mL) purchased from SCP Science. Each plastic tube was then placed into a Thermo Max Q4000 orbital shaker set to 60 rpm and incubated at 40 °C for 24 hours. After incubation, the precipitate containing TiO_2 particles and bound Ag was isolated by centrifugation (6 min, 3900 rpm/3214 rcf) and the supernatant was removed carefully with a pipette. A 20 mL portion of the supernatant was then acidified to 2% HNO_3 and analyzed by ICP-MS to determine the amount of Ag mass in the supernatant (unbound Ag). A water control (no TiO_2) was also run in parallel. In select cases, the TiO_2 precipitate was dried in a vacuum oven, weighed, and then digested in 1.5 mL aqua regia for 48 hrs at room temperature, after which a 1 mL aliquot of the resulting supernatant was diluted to 40 mL and analyzed to determine the amount of Ag bound to TiO_2. The amount of Ag lost to the tube was determined from mass balance between the initial Ag, the amount of Ag in the supernatant, and the amount of Ag bound to TiO_2.

Synthesis of AgNPs and manufacture of AgNP/LDPE films. Hydrophobic AgNPs capable of being incorporated within LPDE were synthesized in water and phase transferred to chloroform using our published method.[17] Dispersion of these AgNPs into LDPE was accomplished using a DSM Xplore 15 mL micro-compounder. Full details on these procedures are included in the Supporting Information section.

Migration experiments. For simulants containing μTiO_2, miniature AgNP/LDPE sachets were prepared with AgNP/LDPE films for Ag migration tests. AgNP/LDPE film was first rinsed for 1 min with purified water to remove dirt and any polymer debris or dislodged NPs on the film surface and then dried with a Kimwipe. The sachets were manufactured by sealing the film edges with a Midwest Pacific impulse sealer. Each sachet had a width of 26 mm and height of 70 mm. After sachet preparation, one corner of each sachet was cut with a knife and filled with 3 mL of the liquid test medium. The sachet notch was then sealed with tape. Each sachet was fixed onto a tube holder and stored at 40 °C in a Thermo Max Q4000 orbital shaker set to 60 rpm. At the appropriate time point, samples were removed and cooled to room temperature. Samples containing μTiO_2 were transferred to 5 mL Eppendorf centrifuge tubes to separate precipitates (containing μTiO_2 particles and bound Ag) from supernatants (containing unbound Ag^+ or unbound AgNPs) by gentle centrifugation (5000 rpm/2627 rfc, 10 seconds). The supernatants were carefully removed, after which precipitates were digested by adding 1 mL of aqua regia solution,

gently agitating, and incubating for 48 hours at room temperature. The digestate was then diluted 20-fold with purified water before Ag analysis by ICP-MS. The supernatant fraction, containing unbound Ag, as well as samples without μTiO_2 particles, were diluted 20-fold and analyzed both by ICP-MS with 2% (v/v) HNO_3 acidification and SP-ICP-MS without acidification. To minimize environmental contamination due to sampling, independent samples were prepared for each time point rather than aliquot extraction. Four replicates of each condition were performed. Migrated Ag was determined from the measured Ag concentrations using the appropriate dilution factors, the analyzed solution volumes, and the total one-sided contact area of the sachets.

For simulants containing $nTiO_2$, an earlier migration protocol[15] was used that required less AgNP/LPDE film per sample. In this case, 42 mm diameter circles were punched from the AgNP/LDPE film using a hole punch, after which the circles were rinsed to remove debris, dried, and placed in 50 mL polypropylene tubes (Digitubes, SCP science). Simulant (25 mL) was then added to each tube and then the tubes were removed and cooled to room temperature. Samples containing $nTiO_2$ were centrifuged at 3600 rpm (2738 rcf) for 6 min to sediment $nTiO_2$. The simulants were then analyzed for Ag content as described above except that only the supernatants containing sucrose were diluted 20-fold; supernatants without sucrose were simply acidified with nitric acid and assayed directly. Migrated Ag was determined identically to the sachet method except the two-sided film contact area was used.

Inductively Coupled Plasma Mass Spectrometry (ICP-MS) in normal and single particle (SP) mode. ICP-MS was performed on an Agilent (Santa Clara, CA) 8800 triple quadrupole ICP-MS with ASX-500 series autosampler. Total unbound Ag (ionic plus particulate) in the supernatants, bound Ag in the digested precipitates, or unbound Ag in samples without TiO_2 was measured by single quadrupole MS mode. ICP-MS standard solutions were prepared by diluting Ag ions standards (1000 µg/mL) purchased from SCP Science with 2% (v/v) aqueous HNO_3 solution. RF power was set at 1550 W and RF matching was set at 1.8 V. Carrier gas flow was 0.95 L/min. Lenses were autotuned using 1 µg/L tuning solution (Agilent). Sample uptake time was 30 s with 0.5 rpm nebulizer pump speed and 40 s stabilization. Three rinse cycles were run between samples with 2 % (v/v) aqueous HNO_3. The internal standard was 200 µg/L Rh, diluted from a 1000 µg/mL internal standard mix purchased from Agilent. Analyte concentrations were determined using a calibration curve generated from the ratios of the Ag standard signals to

the respective internal standard signals (both in counts per second) for at least four Ag concentration standards spanning the range of 0 (standard blank) to 5 μg/mL. Analytical limits of detection (LODs) and limits of quantitation (LOQs) were determined respectively as 3 and 10 standard deviations above the mean across at least 10 replicate blank solutions.[43] LODs and LOQs varied slightly between ICP-MS runs but were typically in the range of 5-10 and 15-30 ppt (ng/L), respectively. Each run concluded with at least one QC standard on the order of 250 ppt (ng/L) Ag and two verification blanks.

SP-ICP-MS analysis was used to estimate the fraction of total Ag in solution that is particulate (AgNPs). SP-ICP-MS was performed in time-resolved analysis (TRA) mode using an integration time of 3 ms per point. The sample flow rate to the nebulizer was 0.346 mL/min. Sample uptake time was 120 s with 0.1 rpm nebulizer pump speed and 30 s stabilization. Three rinse cycles were run between samples with purified water. To guarantee sizing accuracy, each sample run included at least one quality control (QC) measurement of commercial AgNPs (50 nm, 0.02 mg/mL) purchased from nanoComposix, Inc (NanoXact Silver Nanospheres, product ID AGCN50-50M, lot TJC0163) diluted to 5 ppt (ng/L). Sizing accuracy and concentration was validated with the reference material up to 50 ppt (ng/L), so all SP-ICP-MS measurements were carried out on samples sufficiently diluted so that measured AgNP mass concentrations fell below this threshold. SP-ICP-MS data was analyzed using ICP-MS MassHunter software, v4.2. The particle baseline and detection threshold were determined using the automatic threshold feature to prevent human bias from skewing the particle detection results; MassHunter determines the particle detection threshold as the intersection point of the ionic signal portion and the particle signal portion of the total signal distribution using a proprietary statistical algorithm. The threshold is reported by the software as the background equivalent diameter (BED). Because the BED depends on the ionic background concentration, care must be taken when making quantitative comparisons of particle mass/number concentrations (PNCs/PMCs) or particle size distributions between samples with different background Ag^+ levels (i.e., different BEDs). In this manuscript, it is understood that PNCs and PMCs determined by SP-ICP-MS are lower than the true values and reported particle diameters are higher than the true values. Additionally, all qualitative comparisons of SP-ICP-MS results are made by considering how the BED is likely to influence the reported values; quantitative comparisons are most reliable when the average BEDs determined for two sample groups are statistically indistinguishable.

Statistical analysis. All ICP-MS experiments were conducted in triplicate (Ag-TiO_2 interaction studies, Ag migration experiments with circles) or quadruplicate (sachet migration experiments) with each replicate being completely independent of all other replicates. Sachets that showed signs of leakage were discarded, reducing the number of replicates for those sample sets. On a few occasions, experimental Ag concentrations in migration samples were found to be impossibly high, which was attributed to contamination. Accordingly, all ICP-MS data sets were assessed for outliers using a Grubbs (extreme studentized deviate) test with a 95% confidence level. Replicate samples that failed this test were discarded as contaminated. Ag concentration data reported in this manuscript are the mean values over the acceptable replicates and error bars represent standard deviations from the mean values. Unless stated otherwise, significant differences between different sample sets are those that satisfy two-tailed Students' *t* tests determined at the 95% confidence level ($p < 0.05$). In these tests, a conservative assumption of unequal variances was made.

In certain cases, measured Ag concentrations for specific replicates were either below the determined LOD or above the LOD but below the LOQ. In these situations, we report a range of possible concentrations: if the replicate was below the LOD, the minimum and maximum Ag concentration limits were respectively reported as 0 and the LOD value; if the replicate was above the LOD but below the LOQ, the minimum and maximum Ag concentrations were reported as the LOD and LOQ value, respectively. The range of potential values are represented in Figures as areas with hash marks. No statistical significance comparisons were made for sample sets that contain replicates with concentrations below the LOQ.

Safety statement. No unexpected or unusually high safety hazards were encountered with any of the described experiments.

RESULTS AND DISSCUSSION

Properties of TiO_2. To study Ag-TiO_2 interactions in water and concentrated sucrose solution, as well as assess their impact on AgNP migration, we purchased and characterized two types of TiO_2 that had different primary crystallite sizes. According to the product labels, one of the TiO_2 grades (microcrystalline TiO_2, hereafter called μTiO_2) had a nominal particle diameter of $\approx$1 μm; the other (nanocrystalline TiO_2, hereafter $nTiO_2$) had a nominal particle diameter < 100

nm. Although $nTiO_2$ is more representative of a commercial TiO_2 food additive,[24,44] using both $nTiO_2$ and μTiO_2 allowed us to examine effects of primary TiO_2 crystallite size on photochemical and redox interactions between TiO_2, sucrose, and Ag.

Characterization data for μTiO_2 and $nTiO_2$ are displayed in **Figure 1**. Broad TiO_2 crystallite size distributions for both μTiO_2 and $nTiO_2$ were confirmed by scanning transmission electron microscopy (STEM) imaging (**Figure 1A, 1E**); crystallites of $nTiO_2$ were typically rod-shaped with dimensions ranging from approximately 30-80 nm, whereas most μTiO_2 crystallites were over several hundred μm in size. Darkfield microscope images (**Figure 1B, 1F**) show that both grades of TiO_2 were aggregated, with many aggregates larger than 1 μm; the blue apparent color of $nTiO_2$ (**Figure 1F**) is consistent with the more efficient scattering of short wavelength photons by nanoscale crystallites in this sample. Raman spectroscopy and XRD analysis of the TiO_2 crystal structure indicated the presence of rutile and anatase TiO_2 phases, although the rutile crystal structure was dominant in both samples (**Figure 1C-D** and **1G-H**). Raman and XRD data of $nTiO_2$ both bear hallmarks of nanoscale crystallite dimensions, including a decrease in peak height–to–width ratio of Raman fundamental vibrational modes[45] and broadening of X-ray scattering peaks[25] compared to those of μTiO_2.

TiO_2 hydrodynamic diameters, surface electric properties, and colloidal stability were also examined in both water and 9 wt % aqueous sucrose solution. Representative data are displayed in the Supporting Information, **Figures S1-S3**. In water at 5×10^{-4} wt %, mean hydrodynamic diameters of $nTiO_2$ and μTiO_2 were measured immediately after dispersion and a brief (60 s) sonication to be 702 ± 33 and 2011 ± 67 nm, respectively, indicating extensive particle aggregation regardless of the primary TiO_2 crystallite size (**Figure S1A**). Initially, there was no difference ($p < 0.05$) in the dispersed hydrodynamic sizes of either $nTiO_2$ or μTiO_2 regardless of whether the dispersion medium contained sucrose. However, settling experiments show that both forms of TiO_2 exhibit considerably more long-term colloidal stability in 9 wt % sucrose solution versus in purified water, with $nTiO_2$ exhibiting remarkably little settling over more than 24 hours in the presence of sucrose without agitation (**Figure S3**). During this same time, $nTiO_2$ hydrodynamic diameters in sucrose decreased by about 20% and became more monodisperse, whereas in purified water the average size of unsettled $nTiO_2$ particles exhibited only small changes and the polydispersity increased (**Figure S2**). These experiments suggest that sucrose stabilizes TiO_2

dispersions via a kinetically controlled process, whereas in purified water, TiO_2 particles more rapidly flocculate and settle.

The stability of TiO_2 dispersions by sucrose may be explained by the fact that carbohydrates readily adsorb to TiO_2 particles.[36,37,39,46] Chemisorption occurs via condensation reactions between free Ti(IV)-OH groups on TiO_2 surfaces and carbohydrate hydroxyl groups.[46] For sucrose, evidence for a multilayer corona structure has also been reported, in which a sucrose layer directly bonded to the TiO_2 surface is surrounded by a more diffuse, weakly bound layer held together by hydrogen bonds between water and other nearby sucrose molecules.[36] We directly confirmed that both grades of TiO_2 used in our study bind sucrose, in agreement with this prior literature. Thermogravimetric analysis of TiO_2 stored in sucrose solution and then isolated, washed, and dried showed that sucrose displaces water on the TiO_2 surface and forms both strongly and weakly bonded sucrose-TiO_2 complexes that thermally degrade at different temperatures (**Figure S17**). Raman spectroscopy of the same samples (**Figure S18**) revealed peaks corresponding to characteristic sucrose CH_2 bending vibrations that were significantly shifted compared to their positions in pure hydrated sucrose. These vibrations sensitive to changes in the environment around sucrose CH_2OH groups that frequently participate in hydrogen bonding.[47] Raman spectra of TiO_2 incubated with sucrose also showed the disappearance of the TiO_2 surface O-H stretching vibration at 3690 cm^{-1}, consistent with the bonding model described above. These effects scaled with the sucrose concentration and were more pronounced in $nTiO_2$ than in μTiO_2. More detail on these experiments is provided in the Supporting Information.

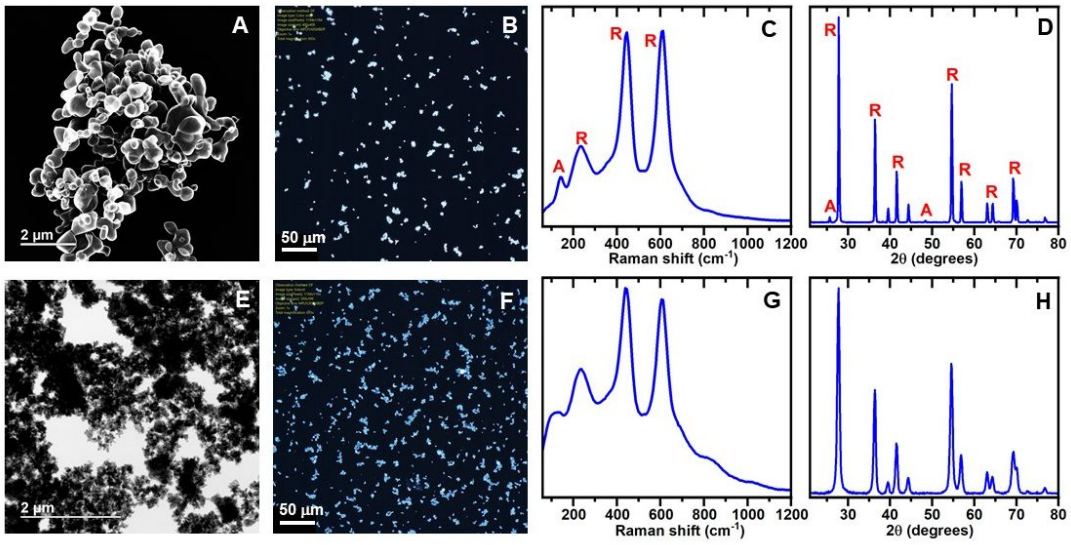

Figure 1. Characterization data for TiO_2 particles. Panels A-D pertain to μTiO_2 and panels E-H pertain to $nTiO_2$. (A, E) STEM images of TiO_2 particles showing a wide distribution of crystallite diameters and confirming the significantly smaller primary crystallite size of $nTiO_2$ with respect to μTiO_2. (B, F) Darkfield microscope images showing that both grades of TiO_2 are aggregated. Raman spectra and X-ray diffractograms of TiO_2 particles are shown in (C, G) and (D, H), respectively. Several characteristic Raman[48] and XRD[25] peaks of rutile and anatase TiO_2 are labeled as R and A, respectively, in (C) and (D)

Interactions between TiO_2 particles, Ag, and sucrose. From the perspective of an Ag-elaborated packaging system, it is important to determine whether migrated Ag exhibits strong interactions with TiO_2 present in the polymer-contacted food matrix, whether these interactions are influenced by other food components, and how such interactions may affect the mass distribution of Ag among its different potential forms (e.g., Ag bound to TiO_2, unbound Ag^+, or unbound AgNPs). To simplify the problem, we first surveyed the landscape of binding interactions between TiO_2 particles and Ag in water or 9 wt % sucrose solution without the complication of a polymeric Ag source. We introduced 500 μM Ag^+ into 0.05 wt % (≈ 0.5 mg/mL) $nTiO_2$ or μTiO_2 aqueous dispersions and then evaluated changes to the dispersions over 10 days during storage at 40 °C (**Figure 2**). A TiO_2 concentration of 0.05 wt % was selected because it is in the middle of the range of TiO_2 concentrations detected in a wide variety of commercial liquid and semi-liquid food and beverage products.[21] An Ag^+ concentration of 500 μM is considerably higher than what would migrate from an AgNP-enabled packaging material, but it facilitates direct visible observation of AgNP formation kinetics.

Time evolution photographs of the samples after brief mixing to resuspend settled particles are displayed in **Figure 2A**. Without TiO_2 (columns labeled ii), there are no color changes evident for Ag^+ stored in water but a remarkable change from clear to orange when Ag^+ is stored in sucrose solution. The orange color is due to AgNPs, as we have reported before.[17] The AgNPs were stable, persisting for over 7 days at 40 °C with little change (other than intensification) to their surface plasmon absorption signatures (**Figure 2B**). As there are no other organic species in solution, the stability of formed AgNPs suggest that sucrose or its downstream hydrolysis/oxidation products are able to act as reasonably effective capping agents, in agreement with prior work on AgNP formation in the presence of sugars.[49,50] Different color changes were observed in samples with $nTiO_2$ (columns labeled iii) and μTiO_2 (iv). Here the emerging color tended to be purple-black and was more intense in samples containing sucrose and in samples containing $nTiO_2$. Photographs of the solutions prior to mixing (Supporting Information, **Figure S4**) demonstrate that the emergence

of purple-black color was correlated with a decrease in the TiO_2 colloidal stability, even when the dispersion medium contained sucrose. Note that the purple-black color is attributed to the settled TiO_2 particles, not the supernatant, although at storage times longer than 1-2 days, a faint orange color consistent with free AgNPs was observed in the supernatants containing both TiO_2 and sucrose. UV-Visible spectroscopy (**Figure 2C**) shows that the concentration of free AgNPs in the sucrose-containing supernatants was higher in μTiO_2 samples than in $nTiO_2$ samples. No evidence of free AgNPs in supernatants was detected in samples without sucrose.

At select time points, XRD and STEM imaging was used to probe the nature of the TiO_2 changes observed in **Figure 2**. XRD analysis of the 10 day precipitates revealed metallic Ag on both $nTiO_2$ (**Figure 2D**) and μTiO_2 (**Figure 2E**), confirming reduction of Ag^+ and binding of the Ag^0 products to the TiO_2 surfaces. In both types of TiO_2, Ag-related XRD peaks were considerably more intense when sucrose was present. This observation signifies that while both $nTiO_2$ and μTiO_2 can reduce ionic Ag by themselves, the process is more efficient in the presence of sucrose. Representative STEM images confirm AgNPs are bound to TiO_2 in both sucrose solution (**Figure 2F**) and purified water (**Figure 2G**). Ag was also confirmed by EDS (**Figure S5**). Note the larger size and higher abundance of AgNPs on the surfaces of μTiO_2 stored in sucrose solution versus purified water, consistent with the XRD results. AgNPs are also found adsorbed on $nTiO_2$ (**Figure S6**), as well as freely dispersed in some regions (i.e., not bound to TiO_2, **Figure S7**), which agrees with the photographic and UV-Vis results (e.g., **Figure 2C**). Freely dispersed AgNPs observed at 4 h were polydisperse, spheroid, and generally < 10 nm in diameter.

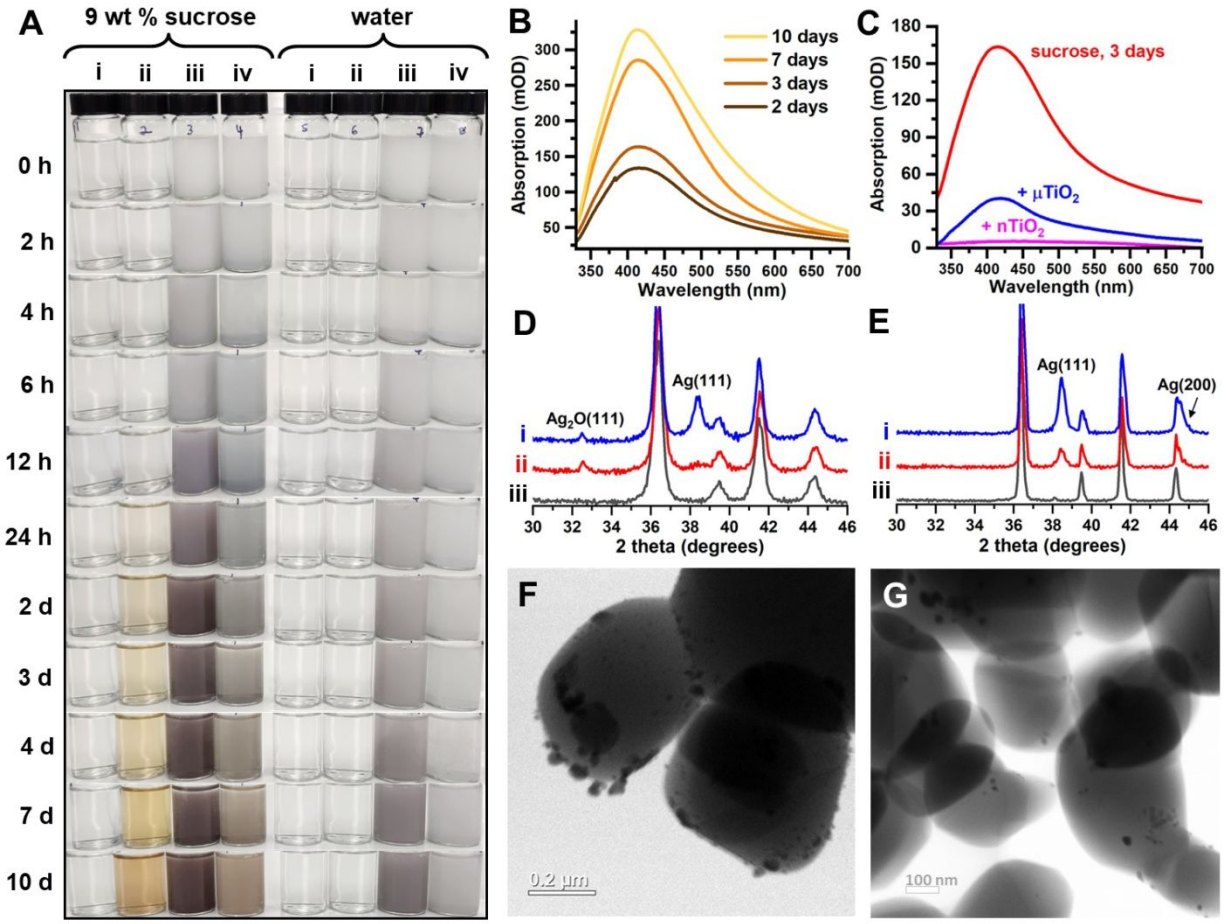

Figure 2. (A) Photographs of 0.05 wt % TiO_2 dispersions in 9 wt % sucrose and purified water as a function of storage time under ambient light at 40 °C: (i) solvent control (no TiO_2 or Ag), (ii) Ag^+ but no TiO_2, (iii) Ag^+ and $nTiO_2$, (iv) Ag^+ and μTiO_2. The Ag^+ concentration was 500 μM. Vials were briefly shaken to distribute TiO_2 before photographing. (B) UV-Visible spectra of 9 wt % aqueous sucrose solutions containing 500 μM Ag^+ at designated times. (C) UV-Visible spectra of 9 wt % aqueous sucrose solutions containing 500 μM Ag^+ and either no TiO_2, 0.05 wt % $nTiO_2$, or 0.05 wt % μTiO_2 (supernatants) after 3 days. (D, E) X-ray diffractograms of (iii, black lines) pristine TiO_2, (ii, red lines) TiO_2 stored in purified water with 500 μM Ag^+, and (i, blue lines) TiO_2 stored in 9 wt % aqueous sucrose solution with 500 μM Ag^+ for 10 days. Diagnostic Ag peaks are indicated. (D) and (E) correspond to $nTiO_2$ and μTiO_2, respectively. XRD spectra over the full angle range are provided in the Supporting Information, **Figure S10**. (F) and (G) show STEM images of 0.05 wt % μTiO_2 after storage with 500 μM Ag^+ in 9 wt % aqueous sucrose solution and water, respectively, for 24 h. The two images are approximately the same magnification scale.

The results in **Figure 2** are consistent with a simple model in which TiO_2 and/or the hydrolysis products of sucrose reduce Ag^+ to Ag^0; Ag^0 then seeds the formation of AgNPs, which have strong affinity for the TiO_2 surfaces. A depiction of this model is shown in **Figure 3**. This process is more efficient for $nTiO_2$ than μTiO_2, either because $nTiO_2$ has stronger redox properties,

more surface area for Ag-TiO_2 interactions, or both. Interestingly, the X-ray diffractograms of $nTiO_2$ showed evidence of both metallic Ag and oxidized Ag_2O, whereas only metallic Ag peaks were observed with μTiO_2 (**Figure 2D, 2E**). The presence of Ag_2O suggests that in addition to mediating Ag^+ reduction, $nTiO_2$ can also facilitate re-oxidation of surface-bound Ag. The amount of Ag_2O relative to Ag on $nTiO_2$ appeared to be higher without sucrose, as signaled by the $Ag_2O(111)/Ag(111)$ peak intensity ratios. We interpret this to mean that in addition to enhancing the Ag^+ reduction, sucrose also protects AgNPs from re-oxidation and dissolution once they are formed, possibly by being a sacrificial hole acceptor.[50,51] This conclusion is supported by STEM images that show that, between 4 h and 24 h, there is an apparent decrease in the number of AgNPs bound to TiO_2 surfaces when the experiment is conducted in water, but an increase in both the number and size of bound AgNPs when the same experiment was conducted in 9 wt % sucrose solution (**Figure S8**). We have also observed that vials containing both TiO_2 and sucrose gradually became bloated during storage under ambient lighting (**Figure S9**), signifying photo-oxidation of sucrose near the TiO_2 surface to carbon dioxide. This is consistent with Vamathevan et al, who studied TiO_2-catalyzed photodegradation of sucrose under various conditions.[41] Accordingly, strong physicochemical interactions between sucrose and TiO_2 may play a role in determining the enhanced production and retention of AgNPs on TiO_2 surfaces when sucrose is present at high concentration.

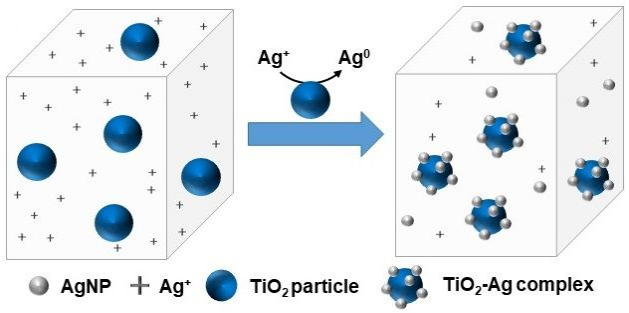

Figure 3. Schematic representation of Ag^+ fate after introduction to an aqueous TiO_2 dispersion. TiO_2 drives Ag^+ reduction to AgNP; a large portion of the total Ag binds to TiO_2 particles to form TiO_2-Ag complexes.

We also examined $nTiO_2$-Ag and μTiO_2-Ag interactions at Ag concentrations in the ppb range, which is similar to Ag levels that have been observed to migrate from AgNP/polymer food storage containers commercially available in Europe.[52] (AgNP/polymer materials are not currently authorized for food contact use in the United States.). In this experiment, either 0.25 or 2.5 ppb

(μg/L) Ag^+ was introduced into 0.05 wt % aqueous TiO_2 particle dispersions and stored for 1 day at 40 °C. ICP-MS was then used to determine the mass fraction of Ag bound to TiO_2 (Ag in a TiO_2-Ag complex, isolated as a precipitate) and the mass fraction of Ag remaining in the supernatant (unbound Ag). Additionally, SP-ICP-MS was used to investigate whether any of the unbound Ag in the supernatant was reduced to AgNPs. The effect of storage in ambient room light and dark conditions was also evaluated. Controls containing no TiO_2 particles were conducted in parallel to examine potential loss of Ag to the storage container surface.

Figure 4A summarizes the Ag mass fractions observed in the supernatant (unbound Ag) after 0.25 ppb Ag^+ was stored in the presence of TiO_2. For $nTiO_2$, unbound Ag was detected in the supernatant in all replicates after storage under both light and dark conditions, but the Ag concentration was below the LOQ. Accordingly, the fraction of unbound Ag was determined to be in the range of 7.5 – 12.2%. The complimentary precipitate analysis (**Figure S11A**) confirms that most of the Ag lost from the supernatant is bound to $nTiO_2$, with no statistical difference between light and dark conditions. Total Ag recoveries after reaction of 0.25 ppb Ag^+ with $nTiO_2$ were calculated to be 100-103% (**Figure S11B**) indicating exceptionally strong Ag-$nTiO_2$ interactions that result in very little Ag loss to the container's polypropylene surface (**Figure S11C**). In contrast, the control experiment showed much lower Ag recoveries (~80%), suggesting that Ag readily binds to plastic when $nTiO_2$ is not present. The analogous experiment with μTiO_2 and 0.25 ppb Ag^+ in the presence of light shows similar results to $nTiO_2$, but in the dark we observed a higher unbound Ag fraction, lower bound Ag fraction, and lower Ag recoveries. These results imply that binding interactions between Ag and μTiO_2 in the dark are weaker than they are under ambient light, weaker than Ag-$nTiO_2$ interactions in either the dark or the light, and competitive with interactions between Ag and the polypropylene tube surfaces. Generally similar results were observed when these experiments were repeated at 10-fold higher (2.5 ppb) Ag^+ concentration (**Figure 4B**), except here the weaker binding capacity of μTiO_2 vis-à-vis $nTiO_2$ is more evident, with higher levels of unbound Ag for μTiO_2 compared to $nTiO_2$ under both light and dark conditions. As before, μTiO_2 binds significantly more Ag in the light (unbound Ag fraction 53.1 ± 6.0 %) than in the dark (9.0 ± 1.0 %).

We also used SP-ICP-MS to examine the AgNP vs. Ag^+ distribution in the supernatants (unbound Ag fractions) after 0.25 ppb Ag^+ was introduced to either $nTiO_2$ or μTiO_2. These results

are provided in **Figure S12**. The quantitative utility of SP-ICP-MS is limited by the fact that varying ionic backgrounds make it difficult to rigorously compare mass fractions of AgNPs across different sample sets, since the ionic background determines the minimum detectable AgNP sizes (see background equivalent diameters, BEDs, plotted in **Figure S12C**). Nevertheless, the SP-ICP-MS results do unequivocally show that both $nTiO_2$ and μTiO_2 generate AgNPs under light and dark conditions. By comparison, a negligible number of AgNPs were observed in the control solutions (**Figure S12A**). Importantly, AgNP particle number concentrations (PNCs) were found to be significantly higher in the presence of $nTiO_2$ ($3.6 \pm 1.1 \times 10^6$ particles L^{-1}) than in the presence of μTiO_2 ($0.7 \pm 0.3 \times 10^6$ particles L^{-1}) under light conditions. Since SP-ICP-MS cannot observe particles with diameters below the BED, these PNC values are probably considerably less than the true AgNP concentrations. Still, as both samples had statistically indistinguishable BED values (**Figure S12**), comparisons of the AgNP PNCs in $nTiO_2$ and μTiO_2 dispersions are fair in a relative sense if the size distribution functions are similar. We note that the mean particle diameters measured here (on the order of 60 nm, **Figure S12**) are larger than those measured by electron microscopy when the initial Ag^+ concentration was 500 μM (5-10 nm, **Figure S7**). SP-ICP-MS overestimates the true mean AgNP diameter for the same reason it underestimates the PNC, but the large AgNP sizes reported here likely signify that some fraction of AgNPs which remain dispersed in the supernatant (are not bound to the TiO_2 surfaces) are aggregated.

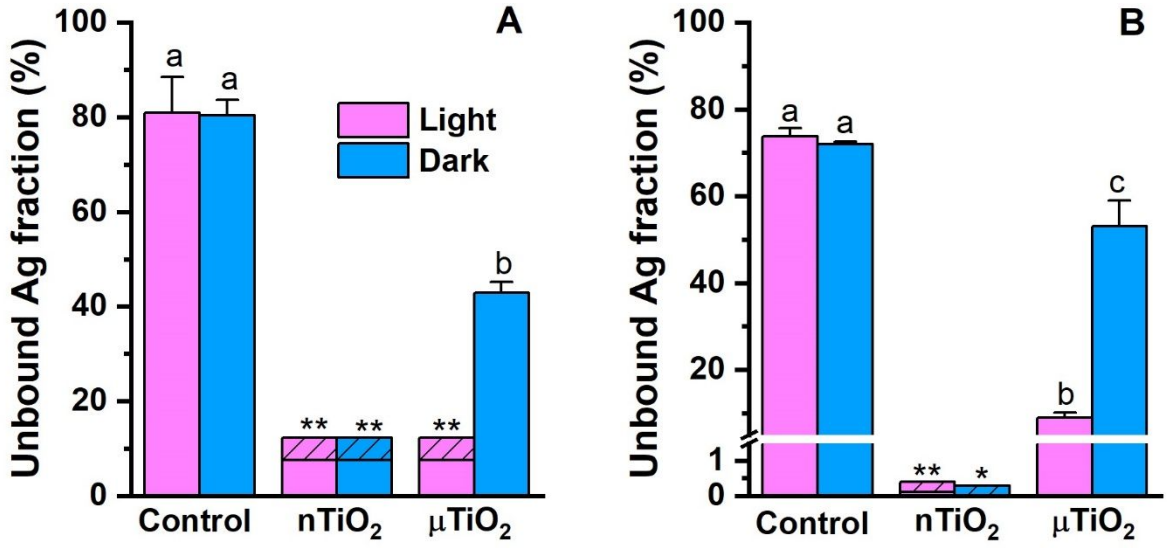

Figure 4. (A) Fraction of Ag remaining in the supernatant phase after 0.25 μg/L Ag^+ and either 0.05 wt% $nTiO_2$ or 0.05 μTiO_2 were stored together in water for 1 day at 40 °C under ambient light and dark conditions. The control sample lacked TiO_2 (Ag^+ in water only). (B) Results for an identical experiment to that shown in panel (A) except the initial Ag^+ concentration was 2.5 μg/L. Bar heights represent average

values over three replicates and error bars represent standard deviations from the mean. Bars indicated by different letters belong to statistically different groups ($p < 0.05$). Single asterisks represent samples in which all three replicates had Ag concentrations below the LOD. Double asterisks represent samples in which at least one replicate was above the LOD but below the LOQ. In these cases, the hashed regions delineate maximum and minimum Ag content, as determined from the LOD and LOQ limits.

Taken together, the Ag-TiO_2 interaction experiments suggest that both $nTiO_2$ and μTiO_2 particles have a strong binding affinity for Ag in water, and these interactions are manifested over a range of Ag concentrations spanning six orders of magnitude (nM to mM). Generally, $nTiO_2$ appears to exhibit stronger (photo)redox properties than μTiO_2, both for driving AgNP formation from dissolved Ag^+ and for re-oxidizing bound AgNPs back to Ag_2O or possibly dissolved Ag^+. Sucrose appears to increase the conversion of Ag^+ to Ag, enhance the binding of Ag to TiO_2, and prevent reoxidation/dissolution of TiO_2-bound Ag. As we'll show, the redox and binding effects of both nanocrystalline and microcrystalline TiO_2 and their interactions with sucrose have implications for the fate of Ag migrated out of AgNP-enabled polymers.

Manufacture of AgNP-loaded LDPE packaging. We prepared miniature AgNP/LDPE sachets and used them to assess Ag migration into TiO_2- and sucrose-containing water in a simulated long-term food/beverage storage application. A photograph of one of these sachets filled with 3 mL of one of the liquid food simulants (9 wt % sucrose and 0.05 wt % μTiO_2) is displayed in **Figure 5A**. AgNP/LDPE sachets were manufactured by first synthesizing hydrophilic, monodisperse AgNPs via reduction of $AgNO_3$ with trisodium citrate dihydrate. Nanoparticle morphology was characterized by STEM (see Supporting Information for details) and a uniform size distribution (mean diameter = 12.8 nm ± 1.4 nm) was observed (**Figure 5B**). The hydrophilic AgNPs were then capped with PEG-2000-SH and phase-transferred from aqueous phase to chloroform phase. AgNP/LDPE cast films were manufactured by melt processing the hydrophobic AgNPs with LDPE and extruding the melt through a heated film die. Sachets were produced from AgNP/LDPE cast films using a heat sealer and filled with 3 mL of liquid food simulant. The Ag concentration in the AgNP/LDPE films was determined by ICP-MS analysis of acid-digested samples to be $2.57 \pm 0.18 \times 10^{-3}$ wt %. Each sachet had an exposed contact area with the simulant (due to partial filling) of 13 cm^2.

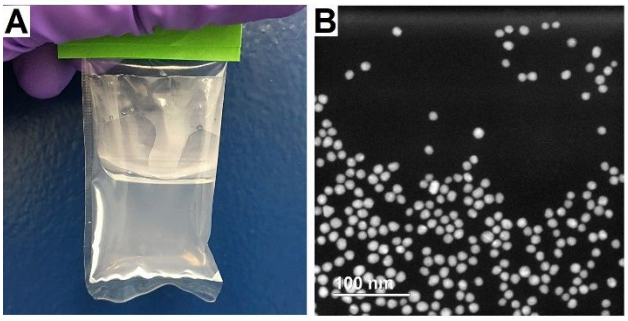

Figure 5. (A) Photograph of a AgNP/LDPE sachet filled with μTiO_2-spiked sucrose solution. (B) STEM image of AgNPs (average size 12.8 nm) in water before phase transfer and dispersion in LDPE.

Effect of TiO_2 particles on Ag migration from AgNP/LDPE packages. Figure 6A summarizes the basic steps in the migration process and how we envisioned – based on our experiments with TiO_2 and Ag in water (**Figures 2-4**) – that TiO_2 could influence Ag migration from AgNP/LDPE packages and into TiO_2-containing foods and beverages in the presence of sucrose. To test this model, we assessed migration from AgNP/LDPE sachets and into water or 9 wt % aqueous sucrose solutions (a concentration typical of sugary beverages, as determined from commercial product nutritional information) charged with different concentrations of μTiO_2 particles under accelerated long term storage conditions (10 days at 40 °C)[53]. Water with sucrose only and water with μTiO_2 only were also assessed to highlight any cooperative effects these two ingredients might have on migration, and water with neither sucrose nor μTiO_2 was used as a frame of reference. After storage, the migrated Ag was speciated with respect to μTiO_2-bound (precipitate analysis) and -unbound fractions (supernatant analysis), and the unbound fraction was also analyzed by SP-ICP-MS. This procedure is illustrated **Figure 6B**. We focused our migration experiments on μTiO_2 because we found $nTiO_2$ difficult to isolate from the aqueous phase without aggressive centrifugation, particularly in the presence of sucrose (see **Figure S3**); in addition, $nTiO_2$ strongly adhered to LDPE contact surfaces, making accurate analysis of migration challenging (see Supporting Information, **Figure S13**). Recognizing that $nTiO_2$ is more representative of TiO_2 that might be used in a food application, however, we also present a limited selection of migration data with $nTiO_2$ at the end of this section.

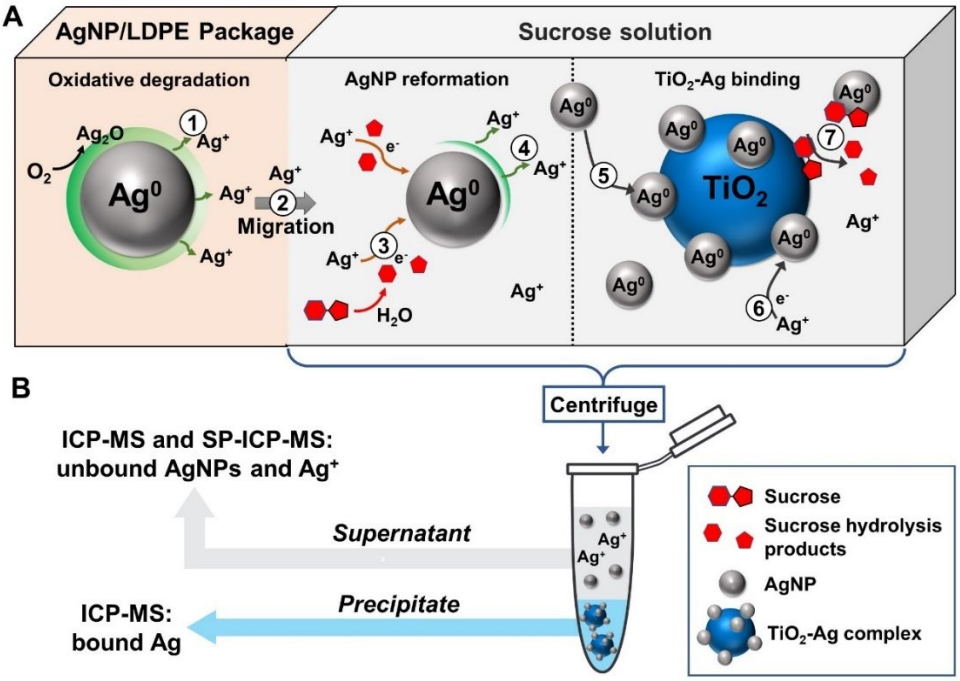

Figure 6. (A) Schematic showing Ag migration from AgNP/LDPE PNCs packaging into sucrose solutions containing TiO_2 particles. The Ag migration and transformation pathway may involve several steps: (1) Polymer-dispersed AgNPs are oxidized by O_2 and release Ag^+. (2) Ag^+ diffuses from the polymer to the surrounding medium. (3) Sucrose slowly hydrolyzes to reducing monosaccharides, which transform migrated Ag^+ into AgNPs. (4) Reformed AgNPs may re-dissolve into Ag^+ and/or (5) adsorb on TiO_2 surfaces. (6) TiO_2 also directly reduces Ag^+ to AgNPs, particularly under room light. (7) TiO_2-sucrose interactions that stabilize TiO_2 particles, reformed AgNPs, and enhance rates of sucrose hydrolysis give rise to cooperative effects on AgNP migration and transformation dynamics. (B) Illustration of sample preparation for ICP-MS and SP-ICP-MS speciation of unbound Ag^+, unbound AgNPs, and bound Ag in aqueous sucrose solution containing TiO_2 particles.

Figure 7A displays total Ag mass migrated from AgNP/LDPE sachets and into aqueous simulants containing (i) 9 wt % sucrose and 0.01 wt% μTiO_2, (ii) 9 wt % sucrose, (iii) 0.01 wt % μTiO_2, and (iv) purified water after storage for 10 days at 40 °C. Speciation of the TiO_2-bound Ag (analysis of precipitate) and unbound Ag (analysis of supernatant) fractions is also indicated for the two samples containing TiO_2. Compared to Ag migration into purified water, we observed significant increases in total Ag migration into all other simulants. The measured dilution-adjusted total Ag concentrations in the simulants at 10 days span a range of approximately 300 to 3000 ppt (ng/L), similar to the Ag concentrations assayed in the Ag-TiO_2 interaction experiments described above. At these levels, total Ag migration typically constitutes 0.05-0.5 % of the initial Ag content within the AgNP/LDPE films. The most migration was observed when the food simulant contained both sucrose and μTiO_2. There was some uncertainty in the total Ag migration into the water control deriving from replicates with concentrations below the LOQ, but if the middle of the range

of potential values in the control (hashed region, **Figure 7A**) is taken as a baseline, the results indicate that migration into water with 0.01 wt % μTiO_2, water with 9 wt % sucrose only, and the combination simulant with both ingredients resulted in approximately 2-fold, 7.8-fold, and 10.3-fold average increases, respectively, in total Ag migration compared to migration into purified water. The particularly high migration into the combination simulant implies that μTiO_2 and sucrose exhibit a cooperative effect on total Ag migration out of AgNP/LDPE packaging.

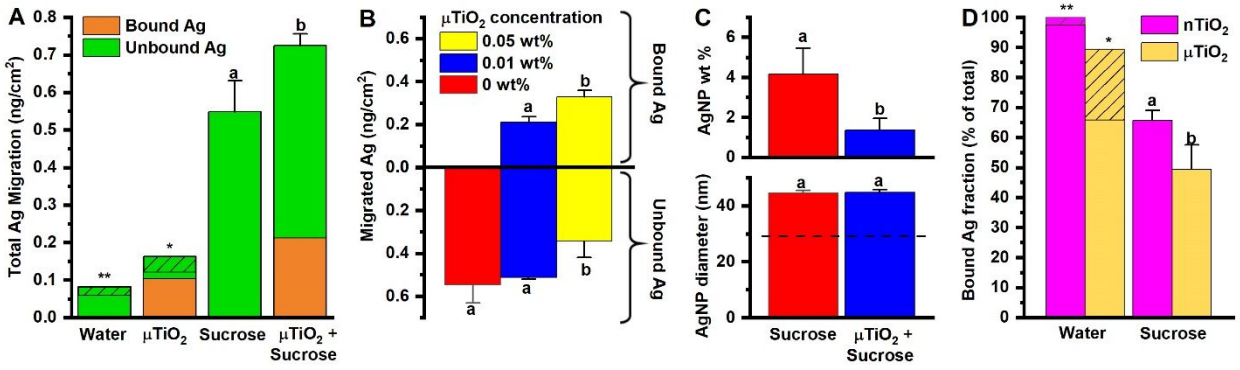

Figure 7. (A) Ag mass migrated (per exposed film surface area) from AgNP/LDPE sachets into four food/beverage simulants containing different combinations of 9 wt % sucrose and 0.1 mg/mL (0.01 wt %) μTiO_2 particles in purified water. Simulants were stored within AgNP/LDPE sachets for 10 days at 40 °C. Each bar differentiates μTiO_2-bound Ag (from the analysis of the μTiO_2 precipitate) and unbound Ag (from analysis of the supernatant). (B) Effect of μTiO_2 concentration on the migration of Ag from AgNP/LDPE sachets into μTiO_2-spiked 9 wt % sucrose solution after 10 days at 40 °C. Bars extending upward represent migrated Ag that is bound to μTiO_2, and bars extending downward represent migrated Ag freely dispersed in the supernatant (unbound). (C) SP-ICP-MS analysis of unbound Ag (supernatant fraction) migrated from AgNP/LDPE sachets into 9 wt % aqueous sucrose solution with or without 0.01 wt% μTiO_2, after 10 days at 40 °C. The top plot shows the fraction (in wt %) of the unbound Ag detected as AgNPs; the bottom plot shows the mean diameters of detected AgNPs. The dashed line indicates the background equivalent diameter (BED) determined from the ionic background. AgNPs with sizes below the BED are not detectable, so the measured AgNP weight fraction underestimates the true AgNP weight fraction. (D) Comparison of the fraction (in wt %) of TiO_2-bound, migrated Ag to the total migrated Ag in purified water or 9 wt % aqueous sucrose solution containing either 0.05 wt % $nTiO_2$ or 0.05 wt % μTiO_2. The migration tests with μTiO_2 used the sachet method and the migration tests with $nTiO_2$ used the circle method (see Materials and Methods for more details). In all cases, bar heights represent mean values determined for 2-4 independent replicates and error bars represent the standard deviations from the mean. Bars indicated by different letters belong to statistically different groups ($p < 0.05$). Single asterisks represent samples in which all three replicates in the supernatant analysis had Ag concentrations below the LOD. Double asterisks represent samples in which at least one replicate was above the LOD but below the LOQ. In these cases, the hashed regions delineate the range of possible Ag content, as determined from the LOD and LOQ limits. Statistical comparisons were not made against sample sets containing replicates with Ag concentration values below the LOQ.

In addition to influencing the total mass of Ag migrating out of AgNP/LDPE materials, μTiO_2 particles and sucrose affected how the migrated Ag mass was distributed among its different

potential forms. The unbound and bound portions of the migrated Ag are indicated in the total Ag migration results in **Figure 7A** and are also plotted independently for each simulant in **Figure S14**. The speciation data for samples containing μTiO_2 indicate that a large portion of the total migrated Ag mass was bound to the μTiO_2 particles (**Figure 7A**). This result is consistent with what was observed when Ag was added directly to aqueous μTiO_2 dispersions and stored for 24 hrs (**Figure 2-4**). The fraction of total migrated Ag that was bound to μTiO_2 was reduced when sucrose was present (29.2 ± 2.0 % versus 69.8 – 89.8 %, **Figure S14C**), even though the total Ag migration was much higher, and the migrated bound Ag increased and unbound Ag decreased as the μTiO_2 concentration increased from 0.01 wt % to 0.05 wt % (**Figure 7B**).

Sub-speciation of the supernatant by SP-ICP-MS was also performed to characterize the distribution of AgNPs and Ag^+ in the unbound portion of the migrated Ag. Select results are provided in **Figure 7C** and additional data in **Figure S15**. AgNPs were observed in all the simulants, including purified water. As before, some caution must be taken in making quantitative comparisons of PNCs or PMCs determined by SP-ICP-MS due to large variations in ionic backgrounds and BEDs across the sample sets. Nevertheless, by placing the calculated PNCs in the context of BED values, there appear to have been the lowest mass concentration of AgNPs in the samples containing only μTiO_2 in water, followed by the purified water control, and then the two samples containing sucrose. The observation of AgNPs in the control is consistent with our earlier work[15,17] and likely derives from direct photoreduction of migrated Ag^+ during the long experimental timescale, whereas the lower AgNP concentration when μTiO_2 was present is in agreement with the strong binding affinity of AgNPs for μTiO_2 demonstrated in experiments described above. The higher PNCs of AgNPs in the sucrose-containing solutions (especially considering the lower detectability of AgNPs in these samples) indicate the efficiency with which sucrose mediates Ag^+ reduction to AgNPs. Notably, the two sample sets containing sucrose had similar particle detection thresholds (statistically indistinguishable BEDs, **Figure S15**), offering a more reliable quantitative comparison of the effect of μTiO_2 on the relative free AgNP concentrations in the supernatant. **Figure 7C** shows that the μTiO_2 reduces the free mass concentration of AgNPs by a factor of more than 3 in sucrose-containing simulants, again demonstrating the strong binding interactions between μTiO_2 and AgNPs. Note that although the sucrose solutions contain the highest AgNP concentrations, AgNPs still only constitute a small (<5

wt % based on detectable particles) portion of the total unbound Ag mass in the supernatant. Presumably, many formed AgNPs become bound to μTiO_2 surfaces. The PMC values in **Figure 7B** are certainly underestimates given the high ionic backgrounds in these samples, but nevertheless it seems likely that most of the migrated Ag mass not bound to μTiO_2 is ionic in form.

The effect of $nTiO_2$ on Ag migration from AgNP/LDPE was also examined. For $nTiO_2$, we employed an immersion-style migration test using punched circles in place of sachets due to a limited supply of AgNP/LDPE film. Loss of $nTiO_2$ to the plastic film surface and difficulty isolating $nTiO_2$ from the aqueous phase likely results in significant underrepresentation of bound Ag in the total Ag migration measurement for sample sets containing $nTiO_2$ and may also result in slight overrepresentation of unbound Ag. Nevertheless, migration results with $nTiO_2$ (**Figure S16**) are generally similar to the μTiO_2 migration results, with the most total Ag migration evident when both $nTiO_2$ and sucrose are present in the simulant. We are unable to make a rigorous quantitative comparison of the total Ag migration observed in simulants containing $nTiO_2$ versus μTiO_2 because migration kinetics in two-sided migration tests are different from those in one-sided migration tests for sufficiently thin films. Even so, the stronger affinity of Ag for $nTiO_2$ is apparent in the plotted bound Ag fractions (**Figure 7D**), which are normalized for the respective total migrated Ag. For instance, in sucrose solution, the fractions of TiO_2-bound Ag to total migrated Ag in the presence of 0.05 wt % $nTiO_2$ and 0.05 wt % μTiO_2 were 65.7 ± 3.3 % and 49.4 ± 8.0, respectively. Thus, while our results cannot establish the effect of TiO_2 crystallite size on total Ag migration from AgNP/LDPE, they do establish that the crystallite size plays a role in determining how the migrated Ag is distributed between bound and unbound forms.

Discussion. The Ag migration results displayed in **Figures 7** and **Figure S16** support the model shown in **Figure 6A**. As we have previously reported, reducing monosaccharides (glucose and fructose) formed when sucrose slowly hydrolyses in purified water catalyze the transformation of migrated Ag^+ into Ag nanostructures exhibiting various morphologies.[17] **Figure 2** showed that sucrose also acts an effective stabilization agent, as AgNPs formed in concentrated sucrose solutions were stable at 40 °C under ambient light and atmosphere for over a week with minimal change to their UV-Vis absorption properties. Vukoje et al has recently revealed that sucrose and other polysaccharides bind to AgNP surfaces and stabilize them by acting as electron donors, which prevents oxidative dissolution of AgNP surfaces and lowers AgNP toxicity compared to

control AgNPs synthesized without carbohydrates.[50] Likewise, Filippo et al synthesized AgNP from maltose and sucrose and concluded that both sugars (and the carboxylic acid products after Ag^+ reduction) act as efficient capping agents that control growth kinetics.[49] In migration tests, the formation and stabilization of AgNPs from Ag^+ migrated out of AgNP/LDPE has the effect of depleting Ag^+ concentrations in the simulant, maintaining a high Ag^+ concentration gradient across the polymer/environment interface, and sustaining a large driving force for Ag^+ diffusion out of the polymer. This is likely why we observe a higher Ag migration into sucrose-containing media than into purified water. TiO_2-catalyzed (photo)reduction of migrated Ag^+ to AgNPs evidently achieves the same endpoint, although to a lesser extent. Also recall that the speciation data in **Figure 7A** and **Figure S16** for samples containing $nTiO_2$ or μTiO_2 indicated that a large portion of the total migrated Ag mass was bound to TiO_2 particles, consistent with what was observed when Ag was added directly to aqueous TiO_2 dispersions (**Figures 2-4**). Ag binding to TiO_2 surfaces would also deplete Ag^+ concentrations in solution, meaning that TiO_2 may exhibit multiple pathways to enhancement of Ag migration out of the polymer.

An especially interesting finding was that sucrose and TiO_2 behave cooperatively in their effect on Ag migration from AgNP/LDPE materials. Total Ag migration into solutions with TiO_2 and sucrose exceeded the migration into simulants containing either of these ingredients alone; also, the migrated Ag in the simulant containing both TiO_2 and sucrose was distributed differently among unbound/bound Ag forms and AgNP/Ag^+ forms than what was observed in either of the single-ingredient simulants. Earlier studies have revealed that carbohydrates bind to metal oxide particles in aqueous media, and such interactions may help explain why sucrose and TiO_2 particles exhibit complex effects on Ag migration when they are present in food simulants simultaneously. For example, Qiaorun et al recently demonstrated that seven common carbohydrates, including sucrose, form dense biocoronas around TiO_2 particles that influence the TiO_2 hydrodynamic diameter, surface charge, and aggregation characteristics in simulated food systems.[36] Glucose,[37,46] dextran,[54] and lactose[51] (among others) have been shown to strongly interact with TiO_2, likely at undercoordinated Ti surface sites. TiO_2 particles are efficient photocatalysts for degradation of surface-bound carbohydrates, including sucrose. Penpolcharoen et al showed that TiO_2 particles not only bind sucrose, but also catalyze sucrose hydrolysis via photoinduced generation of reactive oxygen species,[38] and Kuo et al demonstrated that TiO_2 catalysts efficiently convert adsorbed fructose, glucose, sucrose, and cellulose into various redox-active ketones and esters.[40] Although

the TiO_2 we used in our study has not been engineered for catalytical activity, it is likely that similar surface chemistry occurs, if at lower efficiency; for instance Kuo et al observed chemical transformations of surface-bound carbohydrates even with unmodified commercial TiO_2. We note that these processes would potentially be accelerated when Ag particles are adsorbed on TiO_2, since TiO_2-catalyzed photooxidation of organic substrates has been shown to be enhanced in the presence of AgNPs.[55,56]

This analysis of the prior literature on TiO_2-carbohydrate interactions leads us to speculate that the enhanced Ag migration manifested when TiO_2 and sucrose are both present in the simulant plausibly derives from TiO_2-sucrose binding interactions that: (1) stabilize TiO_2 colloids, reduce TiO_2 homo-aggregation, and increase the efficiency with which TiO_2 both binds and photoreduces Ag^+; and (2) catalyze sucrose hydrolysis, which increases the effective reducing strength of the simulant. Additionally, sucrose likely provides some protection for AgNPs from subsequent photooxidation by TiO_2, possibly as a sacrificial electron donor to photogenerated holes. Both these effects may contribute to enhanced conversion of Ag^+ to AgNP, binding of Ag species to TiO_2 surfaces, and maximizing the concentration gradient across the membrane interface. Our results support all aspects of this model. We observed TiO_2 colloid stabilization in sucrose solution: sucrose reduced TiO_2 particle hydrodynamic diameters (**Figure S2A**), polydispersity indices (**Figures S2B**), and settling rates (**Figure S3**), and TiO_2 particles in sucrose solution had significantly more negative surface charges than in water (**Figure S2C**). We also showed that sucrose strongly binds to TiO_2 surfaces, which is what gives rise to these effects (**Figures S17** and **S18**). We observed significant bloating of reaction tubes when they contained both TiO_2 and sucrose, consistent with CO_2 production due to photodegradation of TiO_2-bound sucrose and possible production of reactive intermediates that may accelerate Ag redox chemistry. Finally, we observed less Ag_2O (relative to metallic Ag) bound to $nTiO_2$ surfaces when sucrose was present, indicating that sucrose suppresses reoxidation of AgNPs after they are formed.

CONCLUSIONS

This study had two important findings. First, we showed that when TiO_2 particles are present at concentrations relevant to their potential use in some foods and beverages, they enhance the transfer of Ag out of AgNP/LDPE packaging materials and into the surrounding environment. TiO_2 particles also convert migrated Ag from ionic to particulate form and efficiently bind to

migrated Ag, thus demonstrating that TiO_2 might influence both the quantity and morphology of Ag in foods or beverages stored within Ag-enabled packaging materials. Second, when sucrose and TiO_2 particles are present in a food or beverage simulant at the same time, the migration of Ag out of AgNP-containing polymers is increased substantially, and sucrose also mediates the fraction of bound versus unbound Ag. This point illustrates that TiO_2 and sucrose exhibit a cooperative effect on the Ag mass transfer dynamics. Additional work needs to be done to clarify the mechanisms underlying Ag-TiO_2-sucrose interactions and their influence on these complicated Ag migration dynamics, but we speculate that this cooperative effect potentially arises due to: binding interactions between TiO_2 particles and sucrose, which stabilize TiO_2 dispersions; and TiO_2-catalyzed sucrose degradation, which may increase the concentration of redox-active substances in the simulant medium. The effect of TiO_2 on Ag migration was true regardless of the TiO_2 crystallite dimensions, although nanocrystalline TiO_2 appeared to possess a larger capacity for binding Ag than microcrystalline TiO_2.

The results presented here provide strong evidence that food and beverage ingredients may influence both the total Ag migration and the distribution of its post-migration transformation products in the event that AgNP-containing polymers are used as packaging materials. Particularly, this work highlights that the highly complex behavior of nanoparticles in even the simplest food systems might have unpredictable effects on migration dynamics. Although this study has focused on TiO_2 and sucrose, it has been well-established that TiO_2 and other metal oxides exhibit strong interactions with a broad range of organic substances in the natural environment[57,58] and in foods.[59-61] This might mean that the migration-enhancing effects demonstrated here may not be limited to sucrose but could be a broader phenomenon characteristic of TiO_2 particles in the presence of other common food substances (proteins, complex carbohydrates, organic acids, etc.). We stress that our migration results cannot be used to make general statements about potential exposure, risk, or safety of AgNP-enabled polymers; determining safety or risk requires additional technical analyses that are beyond the scope of this study and are highly dependent on specific product characteristics and intended use conditions. Nevertheless, the fact that common substances like sucrose and TiO_2 significantly enhance migration of redox-active nanoparticulate polymer additives does suggest that the practice of using simple food simulants (like purified water) may in certain cases underpredict the amount of these additives likely to be found in foods stored in contact with this class of materials.

ACKNOWLEDGMENTS

This work was funded by the United States Food and Drug Administration. TY and LA acknowledge postdoctoral training fellowships awarded through the Oak Ridge Institute for Science and Education (ORISE). ORISE is an asset of the United States Department of Energy. This work made use of the BioCryo facility of Northwestern University's NUANCE Center, which has received support from the SHyNE Resource (NSF ECCS-2025633), the IIN, and Northwestern's MRSEC program (NSF DMR-1720139).

Supporting Information Available: Details on XRD, DLS, STEM, and other T_IO_2 characterization methods, AgNP synthesis procedures, and polymer processing techniques, AgNP characterization data, additional plots of speciated migration data

REFERENCES

1. T. V. Duncan, Applications of nanotechnology in food packaging and food safety: Barrier materials, antimicrobials and sensors*, J. Colloid Interface Sci.*, 2011, **363**, 1-24.
2. J. Sarfraz, T. Gulin-Sarfraz, J. Nilsen-Nygaard and M. K. Pettersen, Nanocomposites for Food Packaging Applications: An Overview*, Nanomaterials*, 2021, **11**, 10.
3. N. Bumbudsanpharoke, W. Lee and S. Ko, A comprehensive feasibility study on the properties of LDPE-Ag nanocomposites for food packaging applications*, Polym. Comp.*, 2018, **39**, 3178-3186.
4. H. M. C. de Azeredo, Antimicrobial nanostructures in food packaging*, Trends Food Sci. Technol.*, 2013, **30**, 56-69.
5. K. Kraśniewska, S. Galus and M. Gniewosz, Biopolymers-Based Materials Containing Silver Nanoparticles as Active Packaging for Food Applications–A Review*, Int. J. Mol. Sci.*, 2020, **21**, 698.
6. S. Kumar, I. B. Basumatary, H. P. K. Sudhani, V. K. Bajpai, L. Chen, S. Shukla and A. Mukherjee, Plant extract mediated silver nanoparticles and their applications as antimicrobials and in sustainable food packaging: A state-of-the-art review*, Trends Food Sci. Technol.*, 2021, **112**, 651-666.
7. H. M. Fahmy, R. E. Salah Eldin, E. S. Abu Serea, N. M. Gomaa, G. M. AboElmagd, S. A. Salem, Z. A. Elsayed, A. Edrees, E. Shams-Eldin and A. E. Shalan, Advances in nanotechnology and antibacterial properties of biodegradable food packaging materials*, RSC Adv.*, 2020, **10**, 20467-20484.
8. H. Ahari and L. K. Lahijani, Migration of Silver and Copper Nanoparticles from Food Coating*, Coatings*, 2021, **11**, 380.
9. J. C. Hannon, J. P. Kerry, M. Cruz-Romero, S. Azlin-Hasim, M. Morris and E. Cummins, Assessment of the migration potential of nanosilver from nanoparticle-coated low-density

polyethylene food packaging into food simulants, *Food Addit. Contam. A*, 2016, **33**, 167-178.
10. M. Jokar, G. A. Pedersen and K. Loeschner, Six open questions about the migration of engineered nano-objects from polymer-based food-contact materials: a review, *Food Addit. Contam. A*, 2017, **34**, 434-450.
11. M. H. Kim, T.-H. Kim, J. A. Ko, S. Ko, J.-M. Oh and H. J. Park, Kinetic and thermodynamic studies of silver migration from nanocomposites, *J. Food Eng.*, 2019, **243**, 1-8.
12. R. A. Trbojevich, S. Khare, J.-H. Lim, F. Watanabe, K. Gokulan, K. Krohmaly and K. Williams, Assessment of silver release and biocidal capacity from silver nanocomposite food packaging materials, *Food Chem. Toxicol.*, 2020, **145**, 111728.
13. A. Mackevica, M. E. Olsson and S. F. Hansen, Silver Nanoparticle Release From Commercially Available Plastic Food Containers into Food Simulants, *J. Nanoparticle Res.*, 2016, **18**, 5.
14. L. d. O. Morais, E. V. Macedo, J. M. Granjeiro and I. F. Delgado, Critical evaluation of migration studies of silver nanoparticles present in food packaging: a systematic review, *Crit. Rev. Food Sci. Nutr.*, 2020, **60**, 3083-3102.
15. R. G. Weiner, A. Sharma, H. Xu, P. J. Gray and T. V. Duncan, Assessment of Mass Transfer from Poly(ethylene) Nanocomposites Containing Noble-Metal Nanoparticles: A Systematic Study of Embedded Particle Stability, *ACS Applied Nano Mater.*, 2018, **1**, 5188-5196.
16. T. V. Duncan and K. Pillai, Release of Engineered Nanomaterials from Polymer Nanocomposites: Diffusion, Dissolution, and Desorption, *ACS Appl. Mater. Interfaces*, 2015, **7**, 2-19.
17. T. Yang, T. Paulose, B. W. Redan, J. C. Mabon and T. V. Duncan, Food and Beverage Ingredients Induce the Formation of Silver Nanoparticles in Products Stored within Nanotechnology-Enabled Packaging, *ACS Appl. Mater. Interfaces*, 2021, **13**, 1398-1412.
18. N. Hadrup and H. R. Lam, Oral toxicity of silver ions, silver nanoparticles and colloidal silver – A review, *Regulatory Toxicology and Pharmacology*, 2014, **68**, 1-7.
19. Z. Chen, S. Han, S. Zhou, H. Feng, Y. Liu and G. Jia, Review of health safety aspects of titanium dioxide nanoparticles in food application, *NanoImpact*, 2020, **18**, 100224.
20. J. Musial, R. Krakowiak, D. T. Mlynarczyk, T. Goslinski and B. J. Stanisz, Titanium Dioxide Nanoparticles in Food and Personal Care Products—What Do We Know about Their Safety?, *Nanomaterials*, 2020, **10**, 1110.
21. A. Weir, P. Westerhoff, L. Fabricius, K. Hristovski and N. von Goetz, Titanium Dioxide Nanoparticles in Food and Personal Care Products, *Environ. Sci. Technol.*, 2012, **46**, 2242-2250.
22. C. Rompelberg, M. B. Heringa, G. van Donkersgoed, J. Drijvers, A. Roos, S. Westenbrink, R. Peters, G. van Bemmel, W. Brand and A. G. Oomen, Oral intake of added titanium dioxide and its nanofraction from food products, food supplements and toothpaste by the Dutch population, *Nanotoxicology*, 2016, **10**, 1404-1414.
23. J.-H. Lim, D. Bae and A. Fong, Titanium Dioxide in Food Products: Quantitative Analysis Using ICP-MS and Raman Spectroscopy, *J. Agric. Food Chem.*, 2018, **66**, 13533-13540.
24. Y. Yang, K. Doudrick, X. Bi, K. Hristovski, P. Herckes, P. Westerhoff and R. Kaegi, Characterization of Food-Grade Titanium Dioxide: The Presence of Nanosized Particles, *Environ. Sci. Technol.*, 2014, **48**, 6391-6400.

25. W. Dudefoi, H. Terrisse, M. Richard-Plouet, E. Gautron, F. Popa, B. Humbert and M.-H. Ropers, Criteria to define a more relevant reference sample of titanium dioxide in the context of food: a multiscale approach, *Food Addit. Contam. A*, 2017, **34**, 653-665.
26. United States Code of Federal Regulations. Title 21. § 73.575 Titanium dioxide.
27. J. Chen, M. Yu, C. Wang, J. Feng and W. Yan, Insight into the Synergistic Effect on Selective Adsorption for Heavy Metal Ions by a Polypyrrole/TiO2 Composite, *Langmuir*, 2018, **34**, 10187-10196.
28. M.-u. Rehman, W. Rehman, M. Waseem, S. Hussain, S. Haq and M. A.-u. Rehman, Adsorption mechanism of Pb2+ ions by Fe3O4, SnO2, and TiO2 nanoparticles, *Environ. Sci. Pollut. Res.*, 2019, **26**, 19968-19981.
29. J. Seidlerová, I. Šafařík, L. Rozumová, M. Šafaříková and O. Motyka, TiO2-Based Sorbent of Lead Ions, *Procedia Mater. Sci.*, 2016, **12**, 147-152.
30. D. N. Misra, "Adsorption" of silver ions on titanium dioxide, *J. Colloid Interface Sci.*, 1968, **28**, 24-27.
31. Y. Choi, H.-i. Kim, G.-h. Moon, S. Jo and W. Choi, Boosting up the Low Catalytic Activity of Silver for H2 Production on Ag/TiO2 Photocatalyst: Thiocyanate as a Selective Modifier, *ACS Catal.*, 2016, **6**, 821-828.
32. M. R. V. Sahyun and N. Serpone, Primary Events in the Photocatalytic Deposition of Silver on Nanoparticulate TiO2, *Langmuir*, 1997, **13**, 5082-5088.
33. Y. Zhang, L. Qiang, Y. Yuan, W. Wu, B. Sun and L. Zhu, Impacts of titanium dioxide nanoparticles on transformation of silver nanoparticles in aquatic environments, *Environ. Sci. Nano*, 2018, **5**, 1191-1199.
34. D. Guin, S. V. Manorama, J. N. L. Latha and S. Singh, Photoreduction of Silver on Bare and Colloidal TiO2 Nanoparticles/Nanotubes: Synthesis, Characterization, and Tested for Antibacterial Outcome, *J. Phys. Chem. C*, 2007, **111**, 13393-13397.
35. Y. Guo, C. Cheng, J. Wang, Z. Wang, X. Jin, K. Li, P. Kang and J. Gao, Detection of reactive oxygen species (ROS) generated by TiO2(R), TiO2(R/A) and TiO2(A) under ultrasonic and solar light irradiation and application in degradation of organic dyes, *J. Hazard. Mater.*, 2011, **192**, 786-793.
36. Z. Qiaorun, S. Honghong, L. Yao, J. Bing, X. Xiao, D. Julian McClements, C. Chongjiang and Y. Biao, Investigation of the interactions between food plant carbohydrates and titanium dioxide nanoparticles, *Food Research International*, 2022, **159**, 111574.
37. V. Butera, A. Massaro, A. B. Muñoz-García, M. Pavone and H. Detz, d-Glucose Adsorption on the TiO2 Anatase (100) Surface: A Direct Comparison Between Cluster-Based and Periodic Approaches, *Frontiers in Chemistry*, 2021, **9**.
38. M. Penpolcharoen, R. Amal and M. Brungs, Degradation of Sucrose and Nitrate Over Titania Coated Nano-hematite Photocatalysts, *J. Nanopart. Res.*, 2001, **3**, 289-302.
39. R. Yusoff, M. H. Kathawala, L. T. H. Nguyen, M. I. Setyawati, P. Chiew, Y. Wu, A. L. Ch'ng, Z. M. Wang and K. W. Ng, Biomolecular interaction and kinematics differences between P25 and E171 TiO2 nanoparticles, *NanoImpact*, 2018, **12**, 51-57.
40. C.-H. Kuo, A. S. Poyraz, L. Jin, Y. Meng, L. Pahalagedara, S.-Y. Chen, D. A. Kriz, C. Guild, A. Gudz and S. L. Suib, Heterogeneous acidic TiO2 nanoparticles for efficient conversion of biomass derived carbohydrates, *Green Chemistry*, 2014, **16**, 785-791.
41. V. Vamathevan, H. Tse, R. Amal, G. Low and S. McEvoy, Effects of Fe3+ and Ag+ ions on the photocatalytic degradation of sucrose in water, *Catalysis Today*, 2001, **68**, 201-208.

42. B. Jin, G. Yao, X. Wang, K. Ding and F. Jin, Photocatalytic Oxidation of Glucose into Formate on Nano TiO2 Catalyst, *ACS Sustainable Chemistry & Engineering*, 2017, **5**, 6377-6381.
43. D., W. B. Crummett and et al., Guidelines for data acquisition and data quality evaluation in environmental chemistry, *Anal. Chem.*, 1980, **52**, 2242-2249.
44. O. Geiss, J. Ponti, C. Senaldi, I. Bianchi, D. Mehn, J. Barrero, D. Gilliland, R. Matissek and E. Anklam, Characterisation of food grade titania with respect to nanoparticle content in pristine additives and in their related food products, *Food Addit. Contam. A*, 2020, **37**, 239-253.
45. V. Swamy, B. C. Muddle and Q. Dai, Size-dependent modifications of the Raman spectrum of rutile TiO2, *Appl. Phys. Lett.*, 2006, **89**, 163118.
46. G. Kim, S.-H. Lee and W. Choi, Glucose–TiO2 charge transfer complex-mediated photocatalysis under visible light, *Appl. Catal. B*, 2015, **162**, 463-469.
47. M. Mathlouthi and D. Vinh Luu, Laser-raman spectra of d-glucose and sucrose in aqueous solution, *Carbohydr. Res.*, 1980, **81**, 203-212.
48. W. Su, J. Zhang, Z. Feng, T. Chen, P. Ying and C. Li, Surface Phases of TiO2 Nanoparticles Studied by UV Raman Spectroscopy and FT-IR Spectroscopy, *J. Phys. Chem. C*, 2008, **112**, 7710-7716.
49. E. Filippo, A. Serra, A. Buccolieri and D. Manno, Green synthesis of silver nanoparticles with sucrose and maltose: Morphological and structural characterization, *J. Non-Crystalline Solids*, 2010, **356**, 344-350.
50. I. Vukoje, V. Lazić, D. Sredojević, M. M. Fernandes, S. Lanceros-Mendez, S. P. Ahrenkiel and J. M. Nedeljković, Influence of glucose, sucrose, and dextran coatings on the stability and toxicity of silver nanoparticles, *Int. J. Biol. Macromol.*, 2022, **194**, 461-469.
51. I. A. Shkrob, M. C. Sauer and D. Gosztola, Efficient, Rapid Photooxidation of Chemisorbed Polyhydroxyl Alcohols and Carbohydrates by TiO2 Nanoparticles in an Aqueous Solution, *J. Phys. Chem. B*, 2004, **108**, 12512-12517.
52. N. von Goetz, L. Fabricius, R. Glaus, V. Weitbrecht, D. Günther and K. Hungerbühler, Migration of silver from commercial plastic food containers and implications for consumer exposure assessment, *Food Addit. Contam. A*, 2013, **30**, 612-620.
53. R. M. S. Cruz, B. P. M. Rico and M. C. Vieira, in *Food Qual. Shelf Life*, ed. C. M. Galanakis, Academic Press, 2019, DOI: https://doi.org/10.1016/B978-0-12-817190-5.00009-4, pp. 281-301.
54. Y. Li and H. G. Spencer, Adsorption of dextrans on spherical TiO2 particles, *Colloids Surf.*, 1992, **66**, 189-195.
55. E. Szabó-Bárdos, H. Czili and A. Horváth, Photocatalytic oxidation of oxalic acid enhanced by silver deposition on a TiO2 surface, *J. Photochem. Photobiol. A*, 2003, **154**, 195-201.
56. V. Iliev, D. Tomova, L. Bilyarska, A. Eliyas and L. Petrov, Photocatalytic properties of TiO2 modified with platinum and silver nanoparticles in the degradation of oxalic acid in aqueous solution, *Appl. Catal., B*, 2006, **63**, 266-271.
57. B. J. R. Thio, D. Zhou and A. A. Keller, Influence of natural organic matter on the aggregation and deposition of titanium dioxide nanoparticles, *J. Hazard. Mater.*, 2011, **189**, 556-563.

58. M. Erhayem and M. Sohn, Stability studies for titanium dioxide nanoparticles upon adsorption of Suwannee River humic and fulvic acids and natural organic matter, *Sci. Total Environ.*, 2014, **468-469**, 249-257.
59. Y. Sun, T. Zhen, Y. Li, Y. Wang, M. Wang, X. Li and Q. Sun, Interaction of food-grade titanium dioxide nanoparticles with pepsin in simulated gastric fluid, *LWT*, 2020, **134**, 110208.
60. C. Li, R. Zhang, C. Ma, H. Shang, D. J. McClements, J. C. White and B. Xing, Food-Grade Titanium Dioxide Particles Decreased the Bioaccessibility of Vitamin D3 in the Simulated Human Gastrointestinal Tract, *J. Agric. Food Chem.*, 2021, **69**, 2855-2863.
61. K. Luo, Y.-l. Yoon, H. Park, S.-J. Choi and Y.-R. Kim, Effect of organic acids on the morphology and particle size of titanium dioxide (E171) in processed food, *J. Hazard. Mater.*, 2022, **432**, 128666.